Journal of Power Sources 616 (2024) 235129

Contents lists available at ScienceDirect

Journal of Power Sources

journal homepage: www.elsevier.com/locate/jpowsour

The effect of pin-type flow field plate design on the current distribution in a H_2-fed polymer electrolyte fuel cell

Andrea Zaffora [a], Orazio Barbera [b,*], Edoardo Gallo [a], Monica Santamaria [a], Giosuè Giacoppo [b]

[a] Department of Engineering, University of Palermo, Viale Delle Scienze, Ed. 6, 90128, Palermo, Italy
[b] Institute for Advanced Energy Technologies "Nicola Giordano" - CNR-ITAE, Via Salita S. Lucia Sopra Contesse 5, 98126, Messina, Italy

HIGHLIGHTS

- Study of a fuel cell using different pin-type flow field plate designs is carried out.
- Pin-type flow field experiences lower pressure drops than serpentine flow field.
- Current and temperature distribution maps are recorded under several operating conditions.
- Increasing coverage factor and decreasing channel width lead to more homogeneous current distribution.

ARTICLE INFO

Keywords:
Polymer electrolyte fuel cell
Hydrogen
Pin-type flow field
Current distribution
Flow field plate design

ABSTRACT

The flow field plate (FFP) design is a key factor for enhancing the electrochemical performance of Polymer Electrolyte Fuel Cells (PEFCs) through optimal reactants' distribution, low-pressure drops, and efficient water removal. The effect of geometrical features of the pin-type FFP design on the electrochemical performance of a 48 cm^2 H_2-fed Fuel Cell (FC) was assessed through polarization curves recording and current and temperature distribution maps along the electrode active area. The study was performed by changing excess air stoichiometry and cathode relative humidity (RH). Low-pressure drops were measured using pin-type FFPs; regardless of geometrical features, they were one order of magnitude lower than those of a single-channel serpentine FFP. Channel width and number of pins greatly influenced the current distribution along the active area and, consequently, the electrochemical performance of FCs. In particular, the best electrochemical performance was reached at air stoichiometry 4 and cathode RH = 100 % by using FFP with the highest coverage factor (65 %) and the lowest channel width (1 mm). Current distribution maps demonstrated that this FFP geometry led to an almost homogeneous current distribution and efficient water removal also at high current density values. On the contrary, low coverage factor (45 %) and high channel width led to worse electrochemical performances due to an uneven reactants distribution and an inefficient water removal, causing cell flooding.

1. Introduction

Hydrogen-based technologies will be crucial to achieving decarbonization goals worldwide since they play an important role in decarbonizing hard-to-abate sectors such as heavy-duty transport and industries (e.g. aviation and maritime) [1–3].

In this context, hydrogen-fed fuel cells (FCs) are among the clean energy technologies used to reach a sustainable energy future. FCs are electrochemical devices that convert reactants' chemical energy into electrical energy with high efficiency and with only one by-product, i.e. water. In particular, Polymer Electrolyte Fuel Cells (PEFCs) operate at low temperatures, i.e. 70-80 °C, exploiting hydrogen oxidation and oxygen reduction at the anode and the cathode, respectively, using a polymeric membrane as a solid electrolyte to allow the movement of protons, H^+, inside the cell [4,5]. A single module FC is composed of different parts: Flow Field Plate (FFP), Gas Diffusion Layer (GDL), Catalyst Layer (CL), and Proton Exchange Membrane (PEM). GDLs, CLs, and the PEM compose the Membrane Electrode Assembly (MEA), the core of an FC, where the reactions and ionic movement occur. Anyway, among the critical components determining the performance of an H_2-fed FC, the FFP design plays a key role. Several aspects of a proper working operation of FCs are related to the FFP design: i) uniform

* Corresponding author.
E-mail address: orazio.barbera@itae.cnr.it (O. Barbera).

https://doi.org/10.1016/j.jpowsour.2024.235129
Received 3 June 2024; Received in revised form 12 July 2024; Accepted 24 July 2024
Available online 27 July 2024

distribution of hydrogen and oxidant along all the active area through the GDL, possibly with small pressure drop, ii) removal of produced water to prevent cell flooding, iii) providing electronic conductivity to conduct electrons toward the external circuit [6,7]. FFPs are typically made in graphite even if in the last decade metal-based FFPs (e.g. stainless steel, titanium) are going to be used due to several properties, such as high thermal and electrical conductivity, high mechanical strength, low gas permeability, and the possibility of making them through additive manufacturing processes, especially for FC-based, electrical, vehicle applications [7–9].

FFP geometrical design is even more crucial in improving the electrochemical performance of an FC. This is particularly true since the main goal of a FFP design is an optimal and homogeneous internal distribution of current and temperature. It has been proved that heterogeneity in current and temperature distribution leads to lower fuel cell durability, due to non-uniform materials degradation, considering both catalyst degradation and carbon corrosion processes [10–12]. Heterogeneous current distribution along the active area can lead to uneven water production with consequent possible temperature hotspots (leading to membrane drying) or coldspots (leading to local condensation phenomena) reducing electrochemical performance and shortening the lifetime of the PEFC. These possible degradation phenomena are more severe in larger cells, since larger gradients in working conditions can be developed, hindering the scaling-up process.

Typical FFP designs used in PEFC include parallel channels, serpentine, interdigitated and pin-type designs. In a parallel channels FFP, reactants entering the cell through the inlet gas manifold can flow along multiple parallel paths, exiting through the outlet gas manifold. This design is useful to decrease the hydraulic resistance, reducing pressure drops that are needed to maintain a constant gaseous flow rate [13,14]. Although compression costs are reduced, low-pressure drops can also cause a not proper removal of produced water, especially close to the outlet region, blocking channels and causing a heterogeneous distribution of reactants along the active area [9]. The most used FFP design is the serpentine one, which can be single or multiple depending on the number of channels connecting the inlet and outlet sections. Single serpentine design is more appropriate for small active areas, while multiple one is more effective in distributing reactants along larger active areas with a reduction of pressure drops [8]. Although higher pressure drops, i.e. high compression costs, and possible bypass or short circuit of reactants, water removal operation is easier concerning other FFP designs [7]. The interdigitated FFP design is based on a discontinuous path from the inlet to the outlet section with dead-end channels [15]. This design should force gas reactants through the GDL coupled with efficient water removal. It is generally accepted that electrochemical performances with interdigitated FFP designs are better than those using parallel channels but worse than using a serpentine-based FFP [16]. Therefore, polarization curves study approach is not sufficient for designing FFPs for superior performance requiring a comprehensive evaluation that takes into account also how pressure drop and mass transfer are coupled with electrochemical performance. It is noteworthy to mention that applying the principle of field synergy based on improved mass transfer theory can be useful for designing superior performance FFPs [17,18].

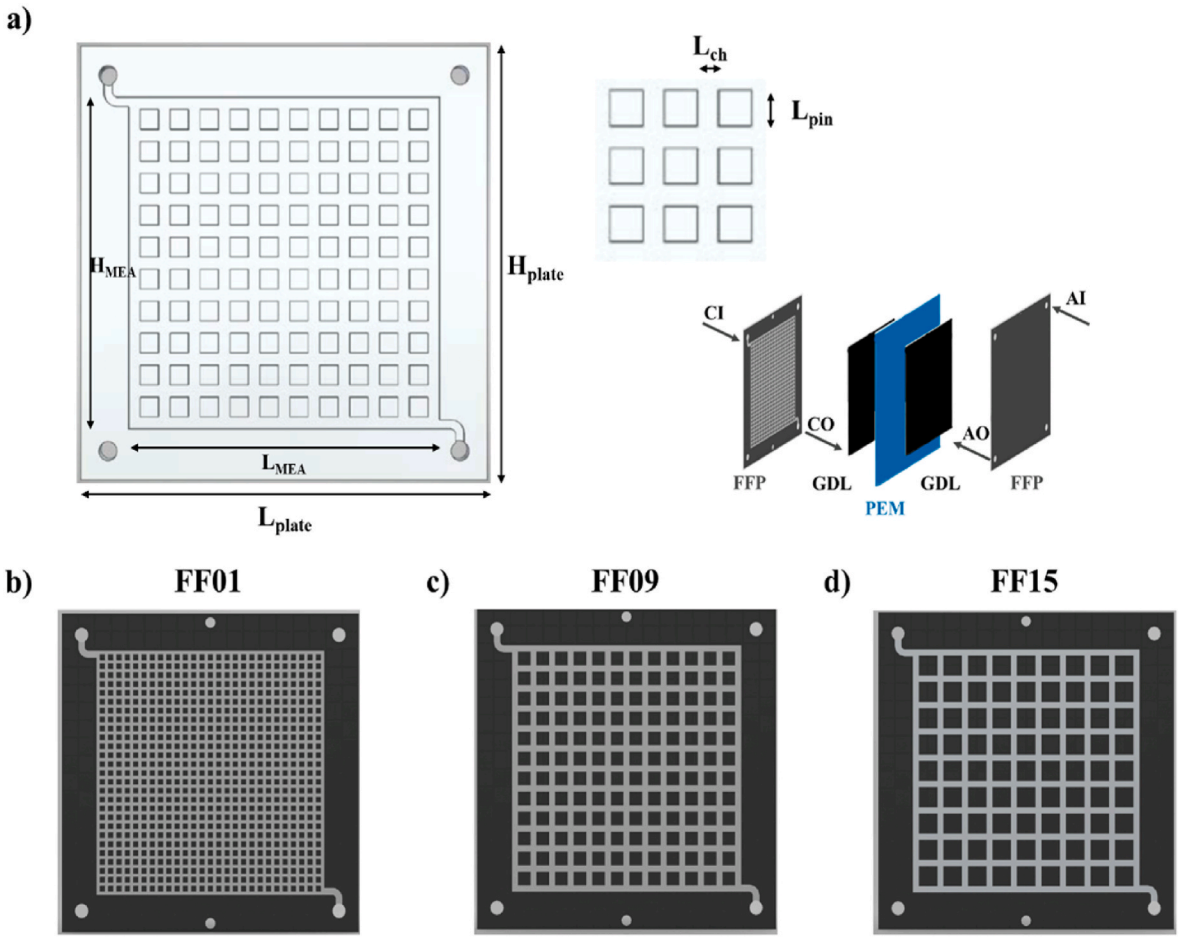

Fig. 1. a) Diagram of the pin-type FFP with an indication of the parameters used for the analytical definition of the geometry and exploded view of a single cell employing pin-type FFPs. Pin-type FFPs with b) 65 % (FF01), c) 55 % (FF09), and d) 45 % (FF15) coverage factor (χ). CI: cathode inlet, AI: anode inlet, CO: cathode outlet, AO: anode outlet.

Among alternative FFP designs, e.g. fractal [19], multi-parallel, bio-inspired [20], radial, tubular [8], pin-type geometry is one of the most studied and used in PEFC applications. This geometry is made by two orthogonal sets of parallel channels created by a domain of square pillars (see below Fig. 1), that allow two-directional reactant flows [9]. The main advantage of this geometry is related to the low-pressure drops, which can be crucial for high-power applications, such as heavy-duty transport. However, gases follow the lowest hydraulic resistance path, usually along the diagonal of the electrode [21], leading to uneven distribution of reactants with stagnant areas and possible water accumulation [9], since many different routes can be followed by the gaseous streams from the inlet to the outlet. Indeed, these issues can lead to low cell efficiency, with lower power density values with respect to those recorded for typical serpentine-based FFP design considering the same flow regimes [22]. Recently, Dang and Zhou studied different types of pin shapes, assessing through Computational Fluid Dynamics (CFD) simulations that diamond-like pins are effective in removing water with low-pressure drops, square-like pins experiment with highest pressure drops removing water very quickly and circle-like pins suffer water accumulation [23]. Other authors designed modified pin-type FFPs to solve the possible flooding issues [24], as using channels with a continuous varying width [21,25]. Despite there are not many experimental studies in literature using pin-type FFP in H_2-fed FCs, it is evident that optimizing FFP geometry can increase electrochemical performances, keeping in mind that, for high-power applications, maintaining low-pressure drops is crucial to lower compression costs.

Here, for the first time, we studied the influence of pin-type geometrical features of an FFP on the electrochemical performance of an H_2-fed PEFC as a function of several operating parameters, such as cathode relative humidity and air stoichiometry. 9 different pin-type FFP designs were tested. Conventional electrochemical characterization through polarization curve recording was then rationalized by current distribution maps, showing how FFP geometry, coupled with the operating conditions, can lead to homogeneous or heterogeneous reactants' distribution and easy/difficult water removal, influencing FC performance. This study provides new insights about pin-type FFP usage, allowing a proper validation of CFD models guiding fuel cell system scale-up for high-power applications.

2. Experimental

2.1. Pin-type bipolar plate design

A pin-type FFP is made by a series of cubical (or cylindrical) pins; ordered in a regular pattern, as shown in Fig. 1a). Therefore, reactants flow through a series and parallel network experiencing a low-pressure drop path. This can lead to an inhomogeneous distribution of reactants and inefficient produced water removal, especially close to the air outlet section.

Geometry is based on a square-shaped active area centered in a square plate of dimensions L_{plate} x H_{plate}. The offset between the active area and plate dimensions forms a flat surface used for the gasket. The chosen shape of the plate is needed to fit the geometrical requirements of the segmented cell device which has A_{MEA} of 48 cm^2 with $L_{MEA} = H_{MEA}$ = 69 mm and $L_{plate} = H_{plate}$ = 90 mm.

The pin is a square pillar providing mechanical support for the MEA, heat, and electrical current conduction. A certain number of pins, N_{pin}, define the geometry of the FFP, i.e. the channels through reactants and products flow during FC operation. As Fig. 1a) shows, a pin is characterized by the length L_{pin}.

The selection of geometries to be adopted and studied was based on the coverage factor, χ, defined as the ratio between the "open" area occupied by the channels, A_{free}, and the total active area referred to the MEA, A_{MEA}. As reported in the literature [7,26], an optimal value for A_{free} parameter is around 50 % of A_{MEA}, corresponding to a good balance between the area directly exposed to the gas and the area available for the electrical conduction of the bipolar plate. Therefore, in this study, χ = 45 %, 55 %, and 65 % (which are directly related to A_{free}) have been examined.

Once L_{MEA} and H_{MEA} have been fixed, they are related as follows:

$$L_{MEA} = H_{MEA} \tag{1}$$

$$A_{MEA} = L_{MEA} \times H_{MEA} \tag{2}$$

In addition, the geometrical characteristics of the pin-type FFP can be completely defined by using the two more independent parameters L_{ch}, the channel width, and N_{pin}, which is imposed as the same in vertical and horizontal directions.

By combining L_{ch} and N_{pin} with L_{MEA} and H_{MEA}, it is possible to define the dependent geometric parameters, in particular: the size of the pin (L_{pin}), as stated assumed as a square, the open area (A_{free}), and the coverage factor ($\chi = A_{free}/A_{MEA}$). Then,

$$L_{pin} = \left(L_{MEA} - \left(N_{pin} + 1\right) \times L_{ch}\right) / N_{pin} \tag{3}$$

$$A_{free} = \left(L_{MEA} \times H_{MEA}\right) - \left(L_{pin} \times N_{pin}\right)^2 \tag{4}$$

$$\chi = \frac{A_{free}}{A_{MEA}} = \left[\left(L_{MEA} \times H_{MEA}\right) - \left(L_{pin} \times N_{pin}\right)^2\right] \Big/ \left(L_{MEA} \times H_{MEA}\right) = 1 - \left(\left(L_{pin} \times N_{pin}\right)^2 \Big/ A_{MEA}\right) \tag{5}$$

At this stage the problem is analytically defined; indeed, A_{MEA}, L_{ch}, and N_{pin} are arbitrarily chosen, and L_{MEA}, H_{MEA}, L_{pin}, A_{free}, and χ are calculated by equations (1)–(5). In summary, there are 8 parameters, 3 are independent, and 5 are calculated from 5 equations.

An Excel spreadsheet has been used to obtain different FFP geometries, by changing channel width, L_{ch}; from 1 to 3 mm with a step of 0.1 mm, N_{pin} from 1 to 31 with a step of 1, and maintaining constant $L_{MEA} = H_{MEA}$ = 69 mm. The procedure generated a table, containing all the values of the found coverage factors, which correspond to a complete set of geometrical parameters of an FFP. In other words, a set of FFPs has been obtained. From the FFP designs' set (see Fig. S1), 18 FFP geometries have been selected, 6 for each coverage factor. (45 %, 55 %, 65 %).

Subsequently, the executive design and manufacturing by graphite milling machining were carried out. It was preferred to accept a small variation in the coverage ratio and impose finite channel widths, following the dimensions of the tool cutters available on the market, to avoid production difficulties.

The tool with a diameter equal to that of the channel passes in the x and y direction generating the pins as a consequence of the machining and the channels of the desired width. This study referred to a geometry that is as simple and easy to implement as possible.

In addition, numerous geometries were obtained that are very similar to each other in terms of coverage factor (χ) but different from the point of view of the fluid dynamic behavior. but different from the point of view of the fluid dynamic behavior.

The selected FFPs are expected to produce important changes in fluid dynamics (pressure drop, velocity) and electrochemical behavior (current distribution, temperature). All the characteristics of the FFPs are reported in Table 1.

3 FFP schemes, with three different χ values, are shown in Fig. 1b), c), and 1d) whilst all the investigated FFP schemes are reported in Fig. S2.

Fig. S3 shows, as an example, one of the 18 graphite plates with defined FFP geometry. They were manufactured by CNC milling and made of composite graphite. The plates were 2 mm thick.

2.2. Pressure drop measurements

Pressure drop measurements were carried out using a gas flow meter, two pressure transmitters, and a cell assembled ad hoc for this purpose.

Table 1
Characteristics of all the investigated pin-type FFPs.

	χ (target)	χ (calculated)	N_{pin}	L_{ch} [mm]	L_{pin} [mm]	L_{pin}/L_{MEA} [−]	L_{ch}/L_{pin} [−]
FF01	65	64.69	27	1	1.52	0.022	0.658
FF02	65	64.69	19	1.4	2.16	0.031	0.648
FF03	65	66.06	15	1.8	2.68	0.039	0.672
FF04	65	65.72	12	2.2	3.37	0.049	0.653
FF05	65	65.72	10	2.6	4.04	0.059	0.644
FF06	65	62.95	8	3	5.25	0.076	0.571
FF07	55	55.56	22	1	2.09	0.030	0.478
FF08	55	54.39	15	1.4	3.11	0.045	0.450
FF09	55	56.33	12	1.8	3.8	0.055	0.474
FF10	55	53.60	9	2.2	5.22	0.076	0.421
FF11	55	56.33	8	2.6	5.7	0.083	0.456
FF12	55	57.47	7	3	6.43	0.093	0.467
FF13	45	45.37	17	1	3	0.043	0.333
FF14	45	45.80	12	1.4	4.23	0.061	0.331
FF15	45	45.37	9	1.8	5.67	0.082	0.317
FF16	45	44.51	7	2.2	7.34	0.106	0.300
FF17	45	45.80	6	2.6	8.47	0.123	0.307
FF18	45	45.37	5	3	10.2	0.148	0.294

No current collectors and electric insulators have been used since no electric current flows in the cell during these tests. The cell has a layered assembly, consisting of two clamping plates, a graphite plate with a defined FFP geometry, a silicone sheet to close the cell, and PTFE gaskets. A pressure transmitter was placed at the beginning and the end of the hydraulic line, to measure the inlet and outlet gas pressure. The two transmitters are part of the Wika© CPH6300 portable pressure tester pack, which includes a control unit, wiring, and pressure transmitters with different sensitivity; in this case, a 600 mbar transmitter was used. These transmitters have a measurement accuracy of 0.1–0.2 % full-scale.

Tests have been carried out by feeding N_2 to the cell through a Bronckhorst© gas flow meter and controller. The same FFP type has been used at the anode and cathode. The gas flow rate varied between 0 and 2.5 normal liters per minute (NLPM), with a 0.1 NLPM step, and kept at the same value for an average of 20 s to give the system enough time to settle at a constant pressure drop value. By combining the information logged in the control unit and the gas flow meter, pressure drops vs gas flow curves have been obtained (see below). These tests were also carried out using a single serpentine FFP (see Fig. S4) to have a comparison with a typically used FFP geometry.

2.3. Experimental setup and electrochemical tests

A single cell with an active area of 48 cm^2 was used for this study. A commercial MEA was used, provided by IRD© with the following characteristics: PFSA – 850 EW 20 μm thick membrane, 60 wt% Pt/C and 50 wt% Pt/C respectively at cathode and anode. The Pt loading was 0.1 mg/cm^2 and 0.4 mg/cm^2 at the anode and cathode, respectively. GDLs were 235 μm thick. The same graphite plates with pin-type FFPs were used for both anodic and cathodic compartments. The cell was then composed of PTFE gaskets, current collectors, and clamping plates.

Greenlight© G60 test station was used for all the electrochemical tests; enabling flow rates and all the operating conditions control. For each measurable quantity in the process (except for the mass flows whose control is integrated into the mass flow meter) it is possible to perform a control via software. The Emerald© software in dotation to the test station has a section that allows the user to define controllers for the desired variable.

Polarization curves were collected at 70 °C feeding H_2 as fuel and air as oxidant with no backpressure. Anode stoichiometry was set at 1.5 and RH was set at 50 % for all the electrochemical measurements. 4 different cathode operating conditions were chosen, resulting in 4 polarization curves for each of the tested FFPs: stoichiometry: 2 and 4, RH: 50 % and 100 %.

Before collecting polarization curves, MEA activation was carried out. The activation procedure consisted of a series of consecutive voltage steps, at 0.8 V and 0.3 V, 10 s and 60 s long, respectively. Once the current reached a constant value (a variation of about 0.1 A s^{-1}) activation was completed. Polarization curves were recorded in galvanostatic mode, starting with the Open Circuit Voltage (OCV) condition and with a current step of 5 A (10 s long) until the cell voltage reaches 0.3 V or a lower cell's voltage value. Every point of the polarization curve was the result of three measurements; so that a more accurate polarization curve can be obtained as an average of three consecutive polarization curves.

2.4. Current and temperature mapping collection

Fig. S5 shows the mapping device, a segmented cell "Current Scan 50" fabricated by S++ (S++ Simulation Service, Germany). It was used to collect the cell's electrical and thermal distribution maps under different operating conditions. The segmented cell is divided into 256 squares of 18.6 mm^2 with dots in their center; these dots are the current and temperature sensors. In particular, the cell has 256 (16x16) current sensors and 16 (8x8) temperature sensors with a 48 cm^2 active area. This sensor plate was placed between the graphite plate and the current collector at the cathode, where the oxygen reduction reaction (ORR) occurs. Current and temperature data were collected through CurrentVIEW V5.6.0 software by S++ Simulation Services. This software allows the user to continuously measure current density and temperature distributions, with the selected measurement period of the scan, and to plot them in 3D plots (X, Y, Current/Temperature). The segmented cell is connected through USB ports to the computer where the associated software is installed. The cell was kept at a constant temperature using flat resistors glued to the surface of the clamping plates and two cooling fans (one for each clamping plate), controlled by two thermocouples inserted into anodic and cathodic clamping plates (see Fig. S5 where the complete experimental setup is shown).

3. Results and discussion

3.1. Pressure drop measurements

Results of pressure drop measurements, as a function of gas flow rates and coverage factor, are shown in Fig. 2, for all the investigated pin-type FFPs.

The highest measured ΔP value is about 30 mbar for 2500 mL min^{-1} as flow rate; regardless of coverage factor, i.e. channel's width and number and dimensions of pins. It can be noticed that in each case the highest ΔP value was measured, in every case, with the FFP with the lowest channel width (i.e. FF01, FF07, and FF13 flow fields). Increasing channel width led to lower measured pressure drops that were very close to each other by changing channel width between 1.4 and 3 mm. In particular, for a $\chi = 65$ %, changing channel width did not have a visible effect on the measured pressure drops (see Fig. 2a) while for a $\chi = 45$ % increasing channel width led to slightly lower pressure drops (see Fig. 2c). Anyway, it can be assessed that pin-type FFPs almost offer the same hydraulic resistance to the gas flows when the coverage factor, and thus the number of pins, increases. Pressure drops were measured in the same operating conditions, also for a single serpentine FFP (see Fig. 2d). As expected, also based on the existing literature [24,27], we measured higher pressure drops in the case of the serpentine FFP with respect to pin-type one. Considering FF01 as a representative geometry of pin-type FFPs, at the highest gas flow rate fed into the cell, there is a difference of about one order of magnitude in the pressure drops, resulting in a much higher hydraulic resistance for the single serpentine. In fact, in a serpentine FFP, the feed (and eventually also products) is forced to go along the entire channel length, whilst in pin-type FFPs the gas flows through the flow channels sequence with the lowest hydraulic resistance [25]. Moreover, if the number of pins increases and, consequently,

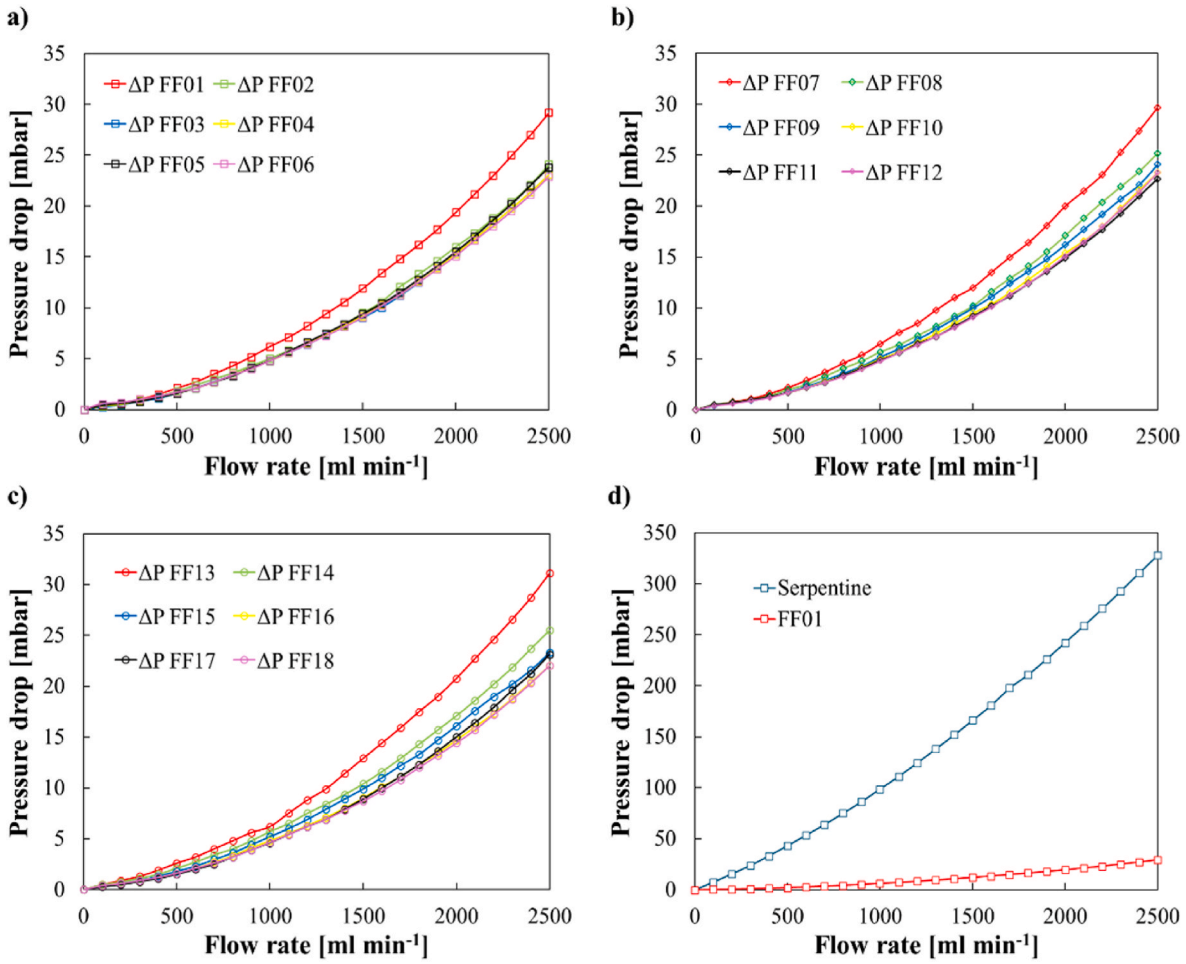

Fig. 2. Pressure drops vs. gas flow rate curves for pin-type FFPs with a) 65 %, b) 55 %, and c) 45 % coverage factor and L_{ch} ranging between 1 mm and 3 mm (see Table 1). d) Comparison of pressure drop vs. gas flow rate curves, measured for FF01 pin-type FFP, and single serpentine FFP.

channel width and pins dimension decrease, the sequence of consecutive pins approach a "wall"-like behavior, thus guiding the reactants through only one direction, reducing the possible flow pathways. This behavior is less accentuated at lower coverage factors since the flow channels are wider and the pins are bigger so that the gas flow has more options in terms of hydraulic pathways.

Once the entire sets of geometries had been hydraulically tested, the most representative pin-type FFPs were electrochemically tested in a single-module fuel cell. Since most of the geometries showed very similar hydraulic performance, it was decided to test three FFPs for each coverage factor value. Particularly, we chose the ones with the highest, intermediate, and lowest channel width value, respectively, for each coverage factor value: FF01, FF03, and FF06 with $\chi = 65$ %, FF07, FF09, FF12 with $\chi = 55$ %, FF13, FF15, FF18 with $\chi = 45$ % (see Fig. S2).

3.2. Electrochemical performances

The effect of pin-type FFPs, and their geometries, on the electrochemical performance of hydrogen-fed FCs was evaluated by recording polarization curves at 70 °C in different operating conditions, i.e. by varying excess air stoichiometry (2 and 4) and cathode RH (50 % and 100 %) and keeping constant anode operating conditions (stoichiometry: 1.5 and RH: 50 %). Interestingly, the results of polarization curves were then rationalized by having a look at the current and temperature distribution along the cathode FFP, which was recorded simultaneously with the recording of polarization curves (see Section 3.3).

Before describing the effect of single geometry of pin-type FFP on the electrochemical performance, we report in Fig. 3 the polarization curves related to FF03 ($\chi = 65$ % and $L_{ch} = 1.8$ mm) and to FF15 ($\chi = 45$ % and $L_{ch} = 1.8$ mm) FFPs, therefore highlighting the effect of χ on electrochemical performances keeping constant L_{ch} value. Results shown for FF03 FFP allows us to discuss the general trend in electrochemical performance as a function of the operating conditions previously described.

In the low current density range, the operating conditions have not influenced the activation region; i.e. on the ORR kinetics. This is anyway due to the lack of a proper and precise mass flow rate control of the experimental equipment in this current range, therefore the air excess concerning the stoichiometric amount is higher in this current region with respect to the other ones, leading to a constant activation voltage loss. The highest effect of operating conditions on the electrochemical performance can be observed by looking at the ohmic region of polarization curves, starting at $\sim$ 0.2 A cm^{-2}. As it is possible to note, the slope of the ohmic region increases by decreasing air stoichiometry and RH, leading to higher ohmic losses. Although, the influence of air stoichiometry seems to be higher than that related to RH value. Ohmic losses are related to electronic and ionic resistance, being the latter the higher contribution of overall ohmic losses due to the membrane resistivity that can highly vary with FC operating conditions [28]. In particular, membrane hydration is crucial to have high ionic conductivity, thus a proper water amount inside the cell is required to maintain the PEM hydrated enhancing cell performance. A higher air stoichiometry leads to a higher water generation due to enhanced ORR kinetics, therefore membrane will be more hydrated. The same effect is caused by

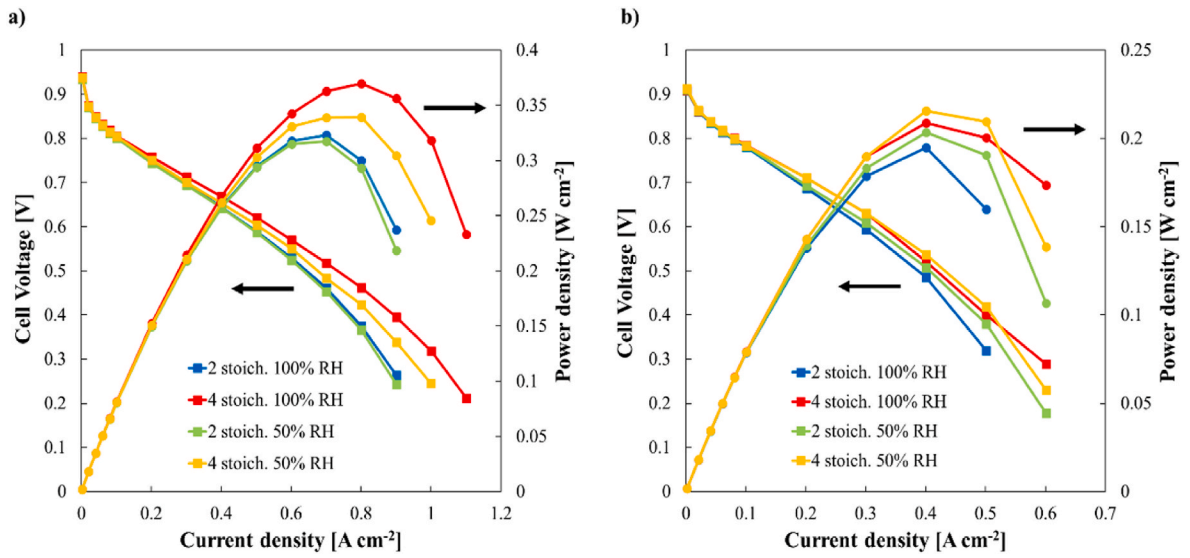

Fig. 3. Voltage vs current density curves recorded at 70 °C in different operating conditions: excess air stoichiometry: 2 and 4 and cathode RH: 50 % and 100 %. Anode stoichiometry: 1.5, RH: 50 %, related to a) FF03 and b) FF15 FFs.

a higher RH since a higher water content in the gas streams ensures good humidification, keeping a higher membrane hydration degree [29,30]. At high current density values, the heat generated because of the reactions inside the cell can lead to membrane drying, decreasing the overall cell performance. A higher RH value can compensate for the tendency of the water evaporation due to the temperature increase, keeping an optimal membrane humidification. Moreover, higher air stoichiometry leads to higher limiting current density values, increasing overall cell performance at high current density. This is why the best performances were reached with the highest tested air stoichiometry (i.e. 4) and the highest tested RH value (100 %) whilst the worst performances were assessed with air stoichiometry 2 and RH = 50 %. The highest power density was recorded with the cell using FF01 (χ = 65 % and L_{ch} = 1 mm), i.e. 520 mW cm^{-2} (see Fig. 4), reaching 1.4 A cm^{-2} at 0.48 V. This behavior was assessed almost for all the tested FFPs, except for those FFPs with bad water management that is directly related to the geometrical features of FFP itself. For instance, in Fig. 3b) we reported polarization curves recorded using FF15 (χ = 45 % and L_{ch} = 1.8 mm)

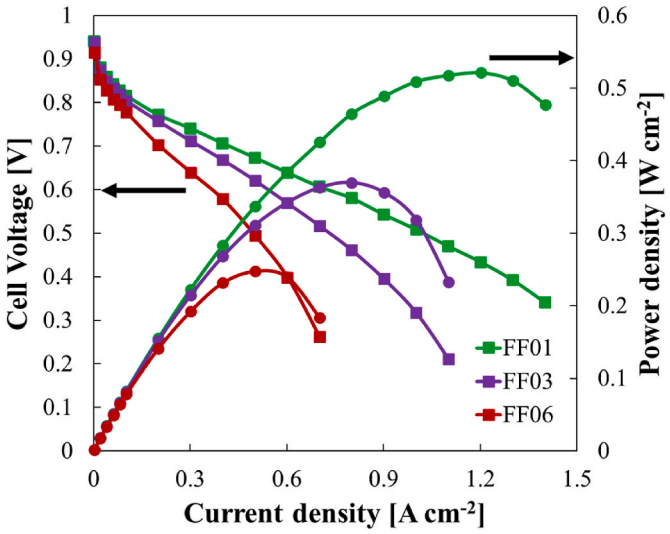

Fig. 4. Voltage vs current density curves recorded at 70 °C with air stoichiometry: 4 and cathode RH: 100 %. Anode stoichiometry: 1.5, RH: 50 %, related to FF01, FF03 and FF06 FFs (χ = 65 %).

with the same operating conditions. Worse cell performances are assessed with respect to the cell with FF03, i.e. FFP with the same L_{ch} and higher coverage factor, determined by a worse reactants' distribution and worse water management, as will be better demonstrated in Section 3.3 by looking at the current distribution maps. Anyway, it is worth noting that the polarization curves are the results of points obtained by time and numerical averages, so the points obtained at high current density can give only a qualitative description of the cell behavior since, at those operating conditions, the cell voltage is often not constant over time but fluctuates with no negligible oscillation amplitudes.

We now compare electrochemical performances of cells operating at the same cathode stoichiometry (i.e. 4) and RH (100 %) varying L_{ch} value (meaning also the number of pins) keeping constant the coverage factor of the FFP. In this regard, polarization curves of cells using FF01, FF03, and FF06 FFs are reported in Fig. 4.

Keeping constant the coverage factor, the higher the number of pins the better the cell performance with the best performance reached by using FF01 whilst the worst performance was assessed by using FF06, reaching 250 mW cm^{-2} as power density peak and only 0.7 A cm^{-2} at 0.26 V. This result, that can be related to higher ionic conductivity of the membrane, is the consequence of a more uniform distribution of the reactants over the entire active area of the electrodes, as assessed by current distribution maps (see below).

Keeping constant channel width L_{ch} and varying the coverage factor leads to similar effects on the electrochemical performance of the FCs, as shown in Fig. 5 where polarization curves recorded using FF01, FF07, and FF13 FFPs are reported in the same operating conditions.

The results showed that when the pins have small dimensions (i.e. for FFPs with 65 % and 55 % coverage factor, FF01 and FF07 in Fig. 5, respectively) geometries with the same channels' width have similar performance; this trend is not confirmed for low coverage factor, i.e. 45 % (FF13 in Fig. 5). Therefore, when the pins have small enough dimensions, polarization curves have similar trends for constant spacing of the pins (channels' width) at high and medium coverage factors; using FFPs with low coverage factor, i.e. bigger pin dimensions, the dependence on the pin geometry is more marked and the performance is worse.

3.3. *Current and temperature distribution along the FFPs*

More insight to better understand electrochemical performance

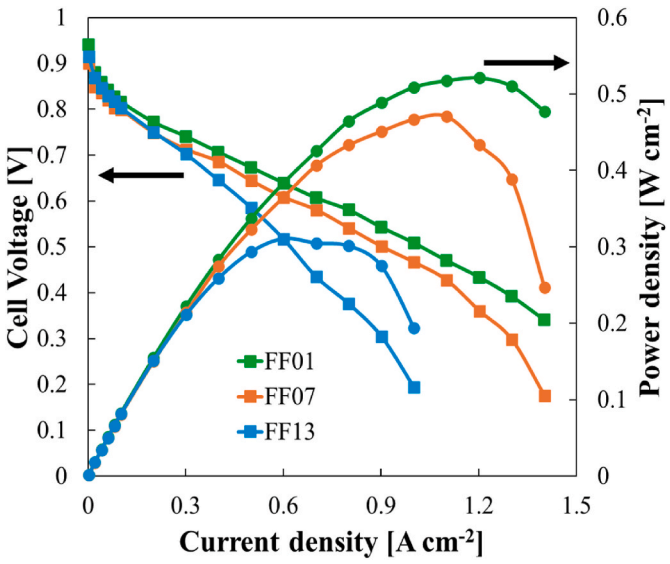

Fig. 5. Voltage vs current density curves recorded at 70 °C with air stoichiometry: 4 and cathode RH: 100 %. Anode stoichiometry: 1.5, RH: 50 %, related to FF01 (χ = 65 %), FF07 (χ = 55 %), and FF13 (χ = 45 %) FFPs.

using the pin-type FFP can be obtained by knowing the current and temperature distribution, along the entire active area. This can be done by reconstructing current and temperature maps of the cathode during cell operation (see Section 2.4), particularly during polarization curves recording. Maps will be shown related to the behavior of the cell in the ohmic region (at 500–600 mA cm^{-2}), at high current density (at 1.3 A cm^{-2}) and, whenever it is possible, in limiting current density region to stress the FFP and assess how the generated water is well or badly managed.

As reported in Section 3.3, best electrochemical performances are reached with air stoichiometry = 4 and RH_C = 100 % by using FF01, (χ = 65 % and L_{ch} = 1 mm). This result can be rationalized by looking at the current distribution maps reported in Fig. 6 recorded at two different operating current densities.

To read and understand the current distribution, it is useful to recall that the cathode inlet and anode inlet are positioned at the top left and top right of the maps, respectively, whilst the cathode outlet and anode outlet are placed at the bottom right and bottom left of the maps, respectively. Generally speaking, uniformly colored maps indicate an even current density distribution. Firstly, it is worth noting that the highest current density area is located near the cathode inlet, regardless of cathode stoichiometry and RH value, whilst the lowest current density area is located at the cathode outlet. This result is not surprising since oxygen partial pressure is crucial to reach high current density conditions, therefore where oxygen partial pressure is still high (near the cathode inlet), the current density will be higher with respect to the area where oxygen partial pressure is lower (near cathode outlet) [31,32]. A higher cathode stoichiometry leads to a more uniform current density distribution for a cell operating at 600 mA cm^{-2}, as it can be possible to notice from the map reported in Fig. 6b) (stoichiometry = 4) concerning that reported in Fig. 6a) (stoichiometry = 2). Then, a lower current density value can be assessed at the cathode outlet for stoichiometry = 2 than that recorded for stoichiometry = 4, indicating a mild initial oxygen starvation condition. Doubling operating overall current density, i.e. 1300 mA cm^{-2}, leads to even more extreme working conditions, shifting the area of high current density closer to the cathode inlet both for air stoichiometry = 2 (see Fig. 6c)) and 4 (see Fig. 6d)), therefore the most active area is located where oxygen partial pressure is still high. As a consequence, the "blue" area is wider, mostly in the stoichiometry = 2 condition (see Fig. 6c)) where the electrode is only partly fully exploited to carry out the reaction leading to a bad usage of the electrode. This behavior is directly related to the pin-type geometry of the FFP, needing higher stoichiometry to work properly when the high current density is drained from the cell. This bad working condition is attenuated by increasing air stoichiometry to 4, as it is possible to note in Fig. 6d), with the cell still operating in the ohmic region, without any oxygen mass transport issue. We can get less information from temperature distribution maps (see Fig. S6) since fewer sensors are present over the electrode active area. Therefore, it is not possible to have a local temperature distribution, but it is still possible to assess the absence of clod and/or hot spots, with an almost uniform temperature distribution, helped by the active cooling system we used to keep the temperature as constant as possible during FC operation.

The effect of FFP geometry keeping a constant coverage factor (χ = 65 %) can be better appreciated in Fig. 7a) and 7b) where current density maps, recorded using FF06 (L_{ch} = 3 mm) at 600 mA cm^{-2} with cathode stoichiometry = 2 and 4 and RH_C = 100 %, are reported.

As already discussed (see Fig. 4), keeping constant the coverage factor and increasing L_{ch} leads to worse electrochemical performances, with a higher slope of the ohmic region of the polarization curve and a lower limiting current density, indicating a not good reactants distribution and water management. This can be explained by looking at the current density maps related to FF01 (Fig. 6a) and b)) compared to those related to FF06 (Fig. 7a) and b)). Despite the local highest current density value being close for the cell operating with different geometry, i.e. 650 mA cm^{-2} and 700 mA cm^{-2} for FF01 and FF06, respectively, current density distribution is completely different. In the case of using the FF06, the high current density area is shifted toward the center of the electrode and the low current density area extends to the top and the right side (toward the anode inlet) of the active area. Therefore, it is possible to assess that increasing L_{ch} leads to a more heterogeneous current density distribution probably due to an uneven reactant distribution. Keeping a constant coverage factor and increasing L_{ch} probably leads to a distribution of reactants along the diagonal of the electrode whilst decreasing L_{ch} leads to a more uniform reactants distribution, extended also to the other parts of the electrode. This result is, anyway, attenuated by the increase in air stoichiometry, as it is possible to notice by the comparison of Fig. 7a) (stoichiometry = 2) and Fig. 7b) (stoichiometry = 4).

Decreasing coverage factor with an intermediate L_{ch} (χ = 55 % and L_{ch} = 1.8 mm) leads to similar results, as it is possible to see from the current density maps related to a cell using FF09 operating at 600 mA cm^{-2}, i.e. high current density area shifted to the center of the electrode and improved reactants distribution by increasing air stoichiometry (see Fig. 7c) and d)). Current density maps can also show the incipient flooding condition, as happens for the cell using FF15 (χ = 45 % and L_{ch} = 1.8 mm) operating at 600 mA cm^{-2} (see Fig. 7e) and f)). The low current density area is quite wide compared to those reported for cells using FFPs with a higher coverage factor, extending from the cathode outlet to the center of the electrode.

One of the main goals of designing a FFP for FCs is its capability in draining reaction products, in our case liquid water from ORR reaction at the cathode. Accumulation of water, or in the worst case, cell flooding, results in a more difficult oxygen supply at the reaction sites in the catalyst layer leading to a lower current density in the electrode areas where produced water accumulates. This phenomenon is of particular importance when the cell operates at high current density, i.e. in operating conditions where a high amount of water is produced. Therefore, we can also use current density maps to assess water management of the different FFPs, with different geometrical features; to understand if the water is or is not correctly drained. Operating conditions that emphasize FFP capability of draining water are air stoichiometry = 4 and RH = 100 % since more oxygen is available for the ORR, also in the cathode outlet region, and because a lower RH leads to possible water evaporation phenomena reducing ionic conductivity and water presence in the GDL. To investigate water management, we report in Videos S1 and S2 related to the temporal evolution of current density distribution along the active

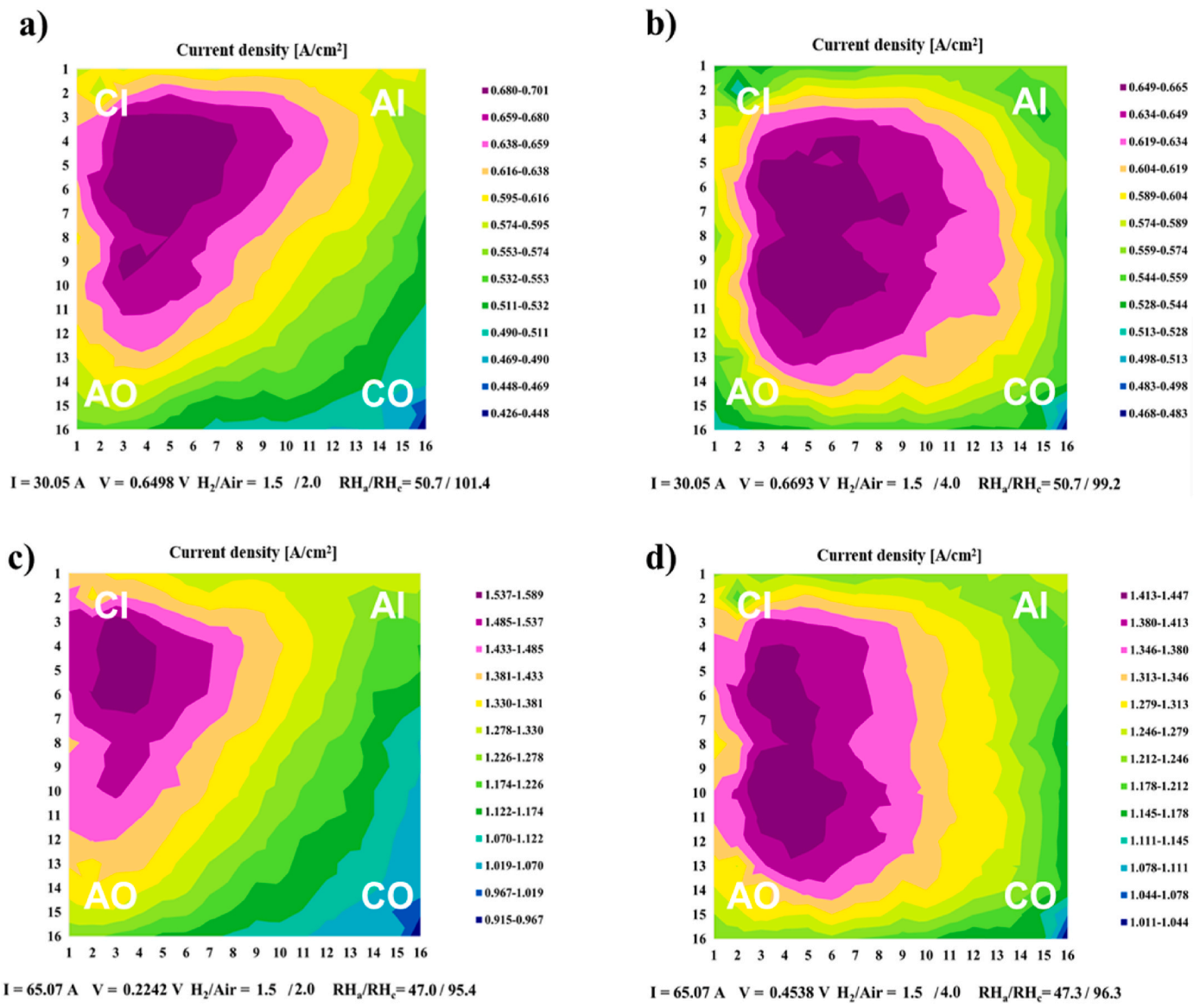

Fig. 6. Current density maps using FF01, at a), b) 600 mA cm^{-2} and c), d) at 1300 mA cm^{-2} with cathode RH = 100 %. a), c): Cathode stoichiometry = 2. b), d): Cathode stoichiometry = 4. Anode stoichiometry: 1.5, RH: 50 %.

area using the FF01 FFP (Video S1), i.e. that one with the best electrochemical performance, and using the FF15 FFP (Video S2), representative of those geometries with intermediate coverage factor (χ = 55 %) but with the highest L_{ch} (3 mm), that produce bad electrochemical performance. In the case of FF01, current density was set to 1400 mA cm^{-2} whilst in the case of FF15 current density was set to 500 mA cm^{-2}. For the sake of convenience, we report in Fig. 8a) and 8b) two current density maps recorded in two moments using the FF01 FFP, doing the same in Fig. 8c) and d) for the cell using the FF15 FFP.

As it is possible to notice in Fig. 8a) and b), the FF01 FFP keeps a good current density distribution over time, with a high current density region near the cathode inlet, with scarce signs of water accumulation, present probably just near cathode outlet region. An opposite behavior can be associated with the cell using the FF15 FFP (see Fig. 8c) and d)), with a higher degree of current density heterogeneity along the entire electrode, with "blue" areas extended almost in all the electrode, a sign of very bad water management with possible water accumulation in the center of the electrode and at the bottom of the electrode, where water can be drained by gravity (see Video S2). This result agrees with the theory, and computational simulations reported in the literature, that FFP geometry influences reactants' distribution, water management, and, therefore, overall electrochemical performance of the entire fuel cell (stack).

4. Conclusions

The influence of geometrical features of a pin-type FFP on the pressure drops and the electrochemical performance of an H_2-fed FC was studied. In particular, 9 different FFPs were studied changing coverage factor and channel width, working under several cathode operating conditions.

The highest pressure drops (i.e. almost 30 mbar at 2.5 L min^{-1} as flow rate) were measured by using the pin-type FFP with the lowest investigated channel width (1 mm), i.e. the highest number of pins, regardless of the coverage factor. These pressure drops value was one order of magnitude lower than that measured using a single-channel serpentine FFP, confirming that pin-type FFP usage leads to low-pressure drops, i.e. lower compression costs.

The best electrochemical performance was reached at air stoichiometry 4 and cathode RH = 100 % by using FF01, i.e. FFP with a

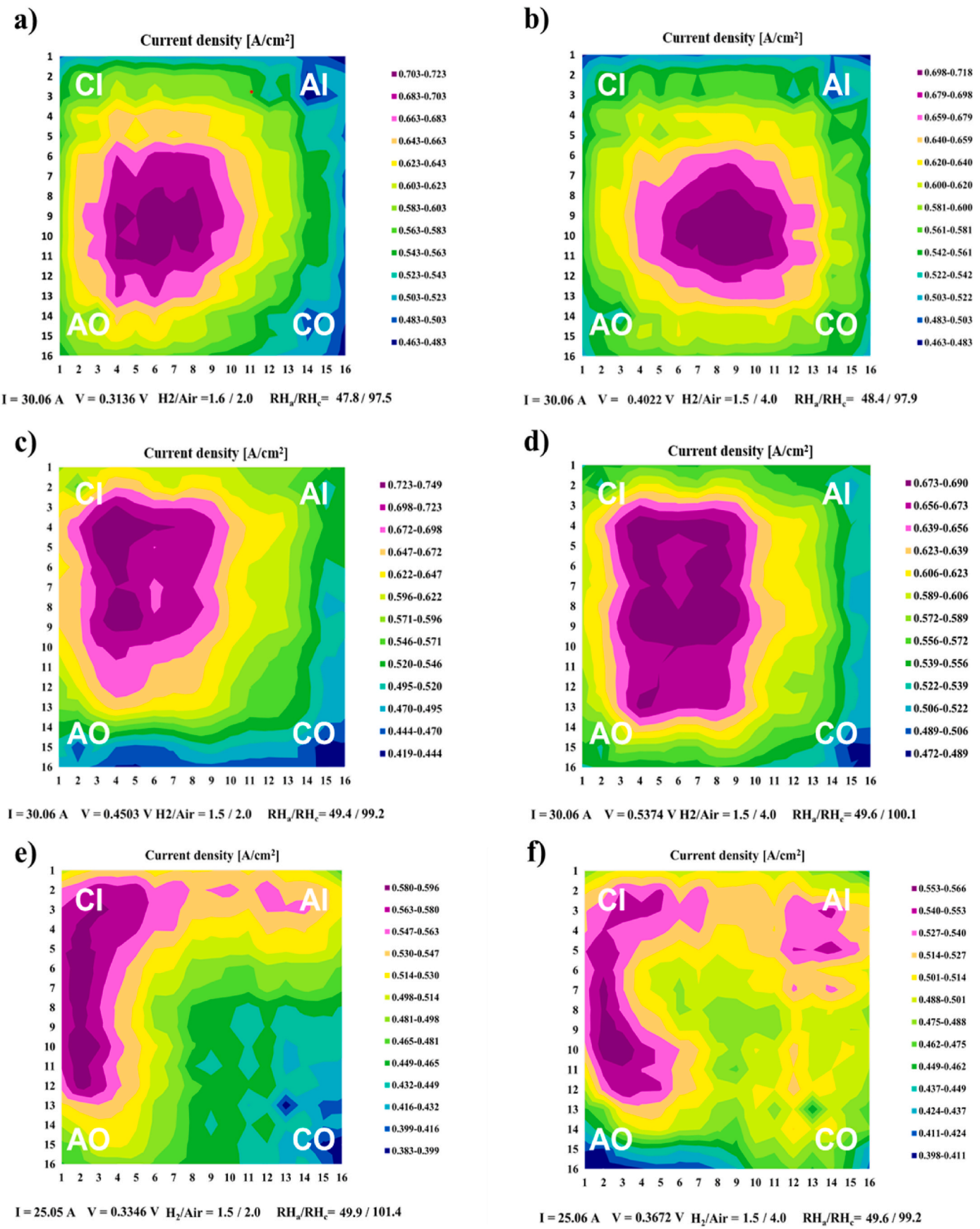

Fig. 7. Current density maps using a), b) FF06, c), d) FF09, and e), f) FF15 FFPs at 500 and 600 mA cm^{-2} with cathode RH = 100 %. a), c), e): Cathode stoichiometry = 2. b), d), f): Cathode stoichiometry = 4. Anode stoichiometry: 1.5, RH: 50 %. CI: cathode inlet, AI: anode inlet, CO: cathode outlet, AO: anode outlet.

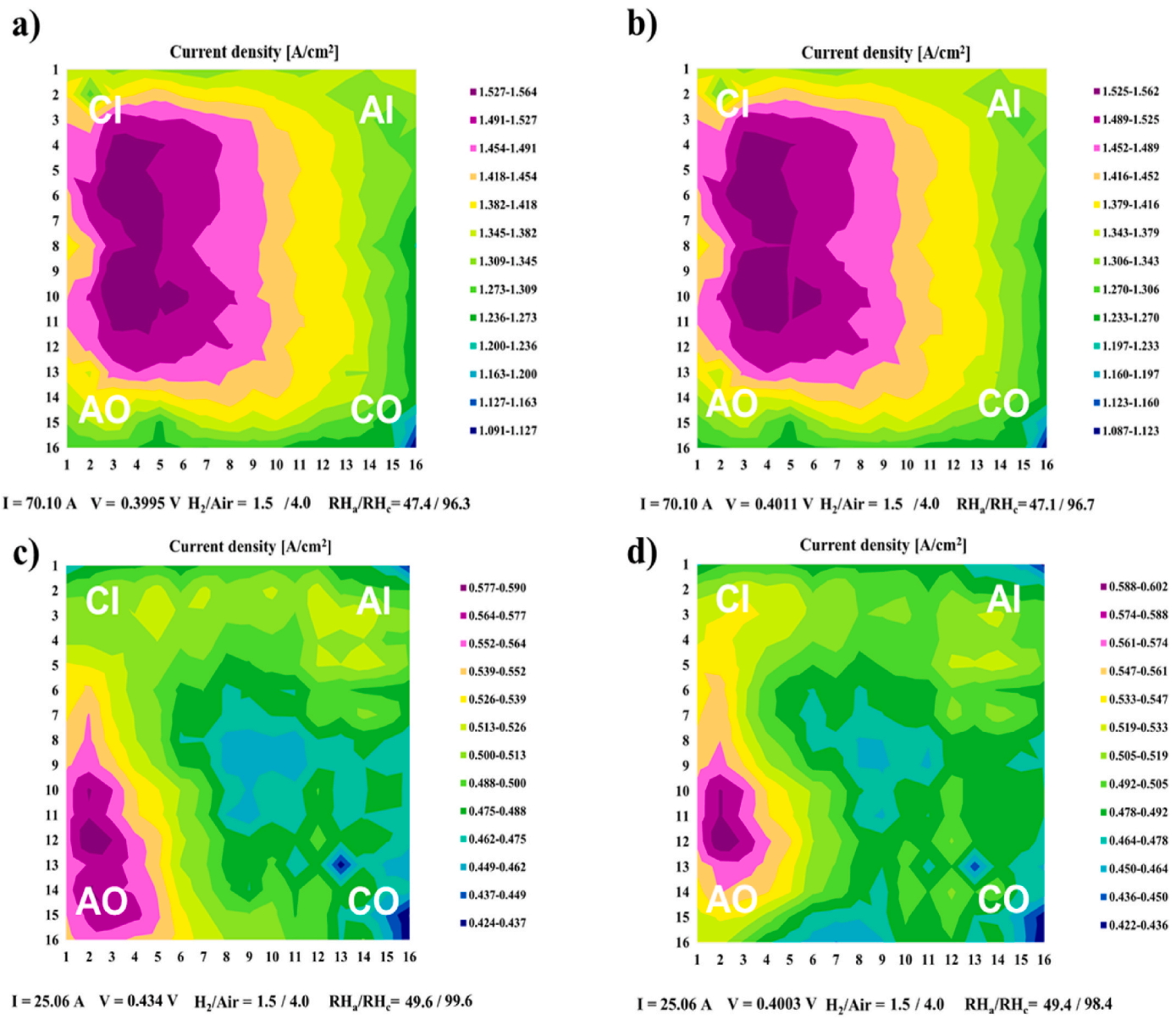

Fig. 8. Current density maps using a), b) FF01 and c), d) FF15 FFPs at 1400 and 500 mA cm^{-2}, respectively, with cathode RH = 100 %, Cathode stoichiometry = 4. Anode stoichiometry: 1.5, RH: 50 %. CI: cathode inlet, AI: anode inlet, CO: cathode outlet, AO: anode outlet.

coverage factor of 65 % and L_{ch} = 1 mm. Considering FFPs with the same coverage factor, a lower channel width caused a higher ionic conductivity of the membrane; a consequence of a more uniform distribution of the reactants over the entire active area of the electrodes, as shown by the recorded current distribution maps. Considering FFPs with different coverage factors and the same channel width, when the pins have small enough dimensions, polarization curves have similar trends at high and medium coverage factors whilst with low coverage factor, i.e. bigger pin dimensions, the dependence on the pin geometry is more marked and the performance is worse.

These results can be rationalized by taking into account the current distribution maps along the entire active area of the electrodes. The high coverage factor and low channel width led to an almost homogeneous current distribution, supposed to be due to an almost uniform reactants distribution related to the peculiar FFP geometry. High air stoichiometry (4) and high RH (100 %) improved the uniformity in operating conditions leading to the best electrochemical performance. On the other hand, increasing L_{ch} leads to a more heterogeneous current density distribution probably due to an uneven reactants' distribution that is collected more along the diagonal of the electrode whilst decreasing L_{ch} leads to a more uniform reactants distribution, extended also to the other parts of the electrode. These geometrical features also helped in draining produced water during working operation at high current density whilst low coverage factor (45 %) and high channel width led to worse reactants distribution and inefficient water removal, also causing cell flooding.

Based on the results of this study, at constant coverage factor, designing a FFP with the highest number of pins leads to more uniformly reactants distribution since gases can follow many hydraulic pathways along the entire active area, although pressure drop can increase. Generally speaking, using pin-type FFP, increasing coverage factor is beneficial for reaching higher electrochemical performance due to a more uniform reactants distribution, proved by more uniform current distribution maps.

Therefore, results proved the potentiality of pin-type FFP design in enhancing electrochemical performance and maintaining low pressure drops, i.e. decreasing compression costs that can be an issue in high-power applications. Moreover, current distribution maps can represent

a suitable and reliable way to validate CFD models.

CRediT authorship contribution statement

Andrea Zaffora: Writing – review & editing, Writing – original draft, Formal analysis. **Orazio Barbera:** Writing – review & editing, Visualization, Supervision, Methodology, Formal analysis, Conceptualization. **Edoardo Gallo:** Writing – review & editing, Investigation, Data curation. **Monica Santamaria:** Writing – review & editing, Supervision, Resources, Methodology. **Giosuè Giacoppo:** Writing – review & editing, Supervision, Methodology, Investigation, Conceptualization.

Declaration of competing interest

The authors declare that they have no known competing financial interests or personal relationships that could have appeared to influence the work reported in this paper.

Data availability

Data will be made available on request.

Acknowledgments

This research work did not receive funding from a specific project; it was supported with the two institutions' funds.

Appendix A. Supplementary data

Supplementary data to this article can be found online at https://doi.org/10.1016/j.jpowsour.2024.235129.

References

[1] N.Z. Muradov, T.N. Veziroğlu, "Green" path from fossil-based to hydrogen economy: an overview of carbon-neutral technologies, Int. J. Hydrogen Energy 33 (2008) 6804–6839, https://doi.org/10.1016/J.IJHYDENE.2008.08.054.

[2] S.J. Davis, N.S. Lewis, M. Shaner, S. Aggarwal, D. Arent, I.L. Azevedo, S.M. Benson, T. Bradley, J. Brouwer, Y.M. Chiang, C.T.M. Clack, A. Cohen, S. Doig, J. Edmonds, P. Fennell, C.B. Field, B. Hannegan, B.M. Hodge, M.I. Hoffert, E. Ingersoll, P. Jaramillo, K.S. Lackner, K.J. Mach, M. Mastrandrea, J. Ogden, P.F. Peterson, D. L. Sanchez, D. Sperling, J. Stagner, J.E. Trancik, C.J. Yang, K. Caldeira, Net-zero emissions energy systems, Science (1979) 360, https://doi.org/10.1126/SCIENCE.AAS9793/ (2018).

[3] T. Capurso, M. Stefanizzi, M. Torresi, S.M. Camporeale, Perspective of the role of hydrogen in the 21st century energy transition, Energy Convers. Manag. 251 (2022) 114898, https://doi.org/10.1016/J.ENCONMAN.2021.114898.

[4] Y. Wang, K.S. Chen, J. Mishler, S.C. Cho, X.C. Adroher, A review of polymer electrolyte membrane fuel cells: technology, applications, and needs on fundamental research, Appl. Energy 88 (2011) 981–1007, https://doi.org/10.1016/J.APENERGY.2010.09.030.

[5] Y. Wang, D.F. Ruiz Diaz, K.S. Chen, Z. Wang, X.C. Adroher, Materials, technological status, and fundamentals of PEM fuel cells – a review, Mater. Today 32 (2020) 178–203, https://doi.org/10.1016/J.MATTOD.2019.06.005.

[6] H. Yan, W. Zhang, Z. Qu, N. Chen, Flow field plate of polymer electrolyte membrane fuel cells: a review, J. Renew. Sustain. Energy 15 (2023), https://doi.org/10.1063/5.0124224.

[7] Y. Zhang, Z. Tu, Flow-field design of the bipolar plates in polymer electrolyte membrane fuel cell: problem, progress, and perspective, Applications in Energy and Combustion Science 17 (2024), https://doi.org/10.1016/j.jaecs.2023.100244.

[8] C. Rocha, T. Knöri, P. Ribeirinha, P. Gazdzicki, A review on flow field design for proton exchange membrane fuel cells: challenges to increase the active area for MW applications, Renew. Sustain. Energy Rev. 192 (2024), https://doi.org/10.1016/j.rser.2023.114198.

[9] M. Sauermoser, N. Kizilova, B.G. Pollet, S. Kjelstrup, Flow field patterns for proton exchange membrane fuel cells, Front. Energy Res. 8 (2020), https://doi.org/10.3389/fenrg.2020.00013.

[10] L. Dubau, L. Castanheira, F. Maillard, M. Chatenet, O. Lottin, G. Maranzana, J. Dillet, A. Lamibrac, J.C. Perrin, E. Moukheiber, A. Elkaddouri, G. De Moor, C. Bas, L. Flandin, N. Caqué, A review of PEM fuel cell durability: materials degradation, local heterogeneities of aging and possible mitigation strategies, Wiley Interdiscip Rev Energy Environ 3 (2014) 540–560, https://doi.org/10.1002/WENE.113.

[11] Y. Jiang, L. Huang, X. Zhang, L. Rasha, D.J.L. Brett, Proton exchange membrane fuel cell performance investigation considering internal heterogeneity of current density – a novel method study, Int. J. Hydrogen Energy 47 (2022) 20205–20217, https://doi.org/10.1016/j.ijhydene.2022.04.107.

[12] K. Khedekar, A. Zaffora, M. Santamaria, M. Coats, S. Pylypenko, J. Braaten, P. Atanassov, N. Tamura, L. Cheng, C. Johnston, I.V. Zenyuk, Revealing in-plane movement of platinum in polymer electrolyte fuel cells after heavy-duty vehicle lifetime, Nat. Catal. 6 (2023) 676–686, https://doi.org/10.1038/s41929-023-00993-6.

[13] E. Hontañón, M.J. Escudero, C. Bautista, P.L. García-Ybarra, L. Daza, Optimisation of flow-field in polymer electrolyte membrane fuel cells using computational fluid dynamics techniques, J. Power Sources 86 (2000) 363–368, https://doi.org/10.1016/S0378-7753(99)00478-4.

[14] J. Lobato, P. Cañizares, M.A. Rodrigo, F.J. Pinar, E. Mena, D. Úbeda, Three-dimensional model of a 50 cm2 high temperature PEM fuel cell. Study of the flow channel geometry influence, Int. J. Hydrogen Energy 35 (2010) 5510–5520, https://doi.org/10.1016/J.IJHYDENE.2010.02.089.

[15] G. Hu, J. Fan, S. Chen, Y. Liu, K. Cen, Three-dimensional numerical analysis of proton exchange membrane fuel cells (PEMFCs) with conventional and interdigitated flow fields, J. Power Sources 136 (2004) 1–9, https://doi.org/10.1016/j.jpowsour.2004.05.010.

[16] D. Spernjak, A.K. Prasad, S.G. Advani, In situ comparison of water content and dynamics in parallel, single-serpentine, and interdigitated flow fields of polymer electrolyte membrane fuel cells, J. Power Sources 195 (2010) 3553–3568, https://doi.org/10.1016/J.JPOWSOUR.2009.12.031.

[17] J. Shen, Z. Tu, S.H. Chan, Enhancement of mass transfer in a proton exchange membrane fuel cell with blockage in the flow channel, Appl. Therm. Eng. 149 (2019) 1408–1418, https://doi.org/10.1016/j.applthermaleng.2018.12.138.

[18] J. Shen, Z. Tu, S.H. Chan, Performance enhancement in a proton exchange membrane fuel cell with a novel 3D flow field, Appl. Therm. Eng. 164 (2020), https://doi.org/10.1016/j.applthermaleng.2019.114464.

[19] V.S. Bethapudi, J. Hack, G. Hinds, P.R. Shearing, D.J.L. Brett, M.O. Coppens, Electro-thermal mapping of polymer electrolyte membrane fuel cells with a fractal flow-field, Energy Convers. Manag. 250 (2021), https://doi.org/10.1016/j.enconman.2021.114924.

[20] T. Chen, S. Liu, S. Gong, C. Wu, Development of bipolar plates with different flow channel configurations based on plant vein for fuel cell, Int. J. Energy Res. 37 (2013) 1680–1688, https://doi.org/10.1002/ER.3033.

[21] N. Guo, M.C. Leu, U.O. Koylu, Network based optimization model for pin-type flow field of polymer electrolyte membrane fuel cell, Int. J. Hydrogen Energy 38 (2013) 6750–6761, https://doi.org/10.1016/j.ijhydene.2013.03.066.

[22] S.S. Hsieh, Y.J. Huang, Measurements of current and water distribution for a micro-PEM fuel cell with different flow fields, J. Power Sources 183 (2008) 193–204, https://doi.org/10.1016/j.jpowsour.2008.04.065.

[23] D.K. Dang, B. Zhou, Effects of pin shapes on gas-liquid transport behaviors in PEMFC cathode, J. Power Sources 557 (2023), https://doi.org/10.1016/j.jpowsour.2022.232584.

[24] H. Kahraman, M.F. Orhan, Flow field bipolar plates in a proton exchange membrane fuel cell: analysis & modeling, Energy Convers. Manag. 133 (2017) 363–384, https://doi.org/10.1016/J.ENCONMAN.2016.10.053.

[25] A. Arvay, J. French, J.C. Wang, X.H. Peng, A.M. Kannan, Nature inspired flow field designs for proton exchange membrane fuel cell, Int. J. Hydrogen Energy 38 (2013) 3717–3726, https://doi.org/10.1016/J.IJHYDENE.2012.12.149.

[26] T. Wilberforce, A.G. Olabi, D. Monopoli, M. Dassisti, E.T. Sayed, M. A. Abdelkareem, Design optimization of proton exchange membrane fuel cell bipolar plate, Energy Convers. Manag. 277 (2023), https://doi.org/10.1016/j.enconman.2022.116586.

[27] A. Ghanbarian, M.J. Kermani, J. Scholta, M. Abdollahzadeh, Polymer electrolyte membrane fuel cell flow field design criteria – application to parallel serpentine flow patterns, Energy Convers. Manag. 166 (2018) 281–296, https://doi.org/10.1016/J.ENCONMAN.2018.04.018.

[28] K.D. Kreuer, On the development of proton conducting polymer membranes for hydrogen and methanol fuel cells, J. Membr. Sci. 185 (2001) 29–39, https://doi.org/10.1016/S0376-7388(00)00632-3.

[29] A.Z. Weber, R.L. Borup, R.M. Darling, P.K. Das, T.J. Dursch, W. Gu, D. Harvey, A. Kusoglu, S. Litster, M.M. Mench, R. Mukundan, J.P. Owejan, J.G. Pharoah, M. Secanell, I.V. Zenyuk, A critical review of modeling transport phenomena in polymer-electrolyte fuel cells, J. Electrochem. Soc. 161 (2014) F1254–F1299, https://doi.org/10.1149/2.0751412jes.

[30] I.V. Zenyuk, P.K. Das, A.Z. Weber, Understanding impacts of catalyst-layer thickness on fuel-cell performance via mathematical modeling, J. Electrochem. Soc. 163 (2016) F691–F703, https://doi.org/10.1149/2.1161607jes.

[31] Y. Yu, X.Z. Yuan, H. Li, E. Gu, H. Wang, G. Wang, M. Pan, Current mapping of a proton exchange membrane fuel cell with a segmented current collector during the gas starvation and shutdown processes, Int. J. Hydrogen Energy 37 (2012) 15288–15300, https://doi.org/10.1016/J.IJHYDENE.2012.07.023.

[32] M. Belhadj, A. Aquino, J. Heng, S. Kmiotek, S. Raël, C. Bonnet, F. Lapicque, Current density distributions in polymer electrolyte fuel cells: a tool for characterisation of gas distribution in the cell and its state of health, Chem. Eng. Sci. 185 (2018) 18–25, https://doi.org/10.1016/J.CES.2018.03.055.